Published OnlineFirst March 2, 2017; DOI: 10.1158/1535-7163.MCT-15-1010

Small Molecule Therapeutics

Molecular Cancer Therapeutics

# Akt Activation Mediates Acquired Resistance to Fibroblast Growth Factor Receptor Inhibitor BGJ398

Jharna Datta[1], Senthilkumar Damodaran[1,2], Hannah Parks[1], Cristina Ocrainiciuc[1], Jharna Miya[1], Lianbo Yu[3], Elijah P. Gardner[1], Eric Samorodnitsky[1], Michele R. Wing[1], Darshna Bhatt[1], John Hays[1,2], Julie W. Reeser[1], and Sameek Roychowdhury[1,2,4]

## Abstract

Activation of FGFR signaling through mutations, amplifications, or fusions involving *FGFR1*, *2*, *3*, or *4* is seen in multiple tumors, including lung, bladder, and cholangiocarcinoma. Currently, several clinical trials are evaluating the role of novel FGFR inhibitors in solid tumors. As we move forward with FGFR inhibitors clinically, we anticipate the emergence of resistance with treatment. Consequently, we sought to study the mechanism(s) of acquired resistance to FGFR inhibitors using annotated cancer cell lines. We identified cancer cell lines that have activating mutations in *FGFR1*, *2*, or *3* and treated them chronically with the selective FGFR inhibitor, BGJ398. We observed resistance to chronic BGJ398 exposure in DMS114 (small-cell lung cancer, *FGFR1* amplification) and RT112 (urothelial carcinoma, *FGFR3* fusion/amplification) cell lines based on viability assays. Reverse-phase protein array (RPPA) analysis showed increased phosphorylation of Akt (T308 and S473) and its downstream target GSK3 (S9 and S21) in both the resistant cell lines when compared with matching controls. Results of RPPA were confirmed using immunoblots. Consequently, the addition of an Akt inhibitor (GSK2141795) or siRNA was able to restore sensitivity to BGJ398 in resistant cell lines. These data suggest a role for Akt pathway in mediating acquired resistance to FGFR inhibition. *Mol Cancer Ther; 16(4); 614–24. ©2017 AACR.*

## Introduction

FGFRs play essential roles in mediating cell proliferation, migration, and survival (1). FGFR belongs to the receptor tyrosine kinase (RTK) family of proteins that also includes EGFR and VEGFR family. The FGFR family is comprised of four receptors, FGFR1, FGFR2, FGFR3, and FGFR4 with 18 known ligands. Ligand binding leads to dimerization and conformational change in the receptor, resulting in phosphorylation of tyrosine kinase domains. The phosphorylated tyrosine residues in turn act as a docking site for FGFR substrate 2 (FRS2), a vital adapter protein in the FGFR signaling cascade. Phosphorylation of FRS2 leads to recruitment of adapter proteins, such as SOS, GRB2, and GAB1, resulting in the activation of downstream MAPK or PI3K–Akt pathways.

Deregulation and activation of FGFR signaling has been identified in multiple cancers that include bladder, lung, biliary, prostate, and breast (1, 2). *FGFR1* amplification has been reported in 20% of squamous cell carcinoma of the lung (3). *FGFR3* mutations are reported in approximately 70% of low-grade urothelial carcinomas (4). In addition to oncogenic fusions involving *FGFR3* in bladder cancers, *FGFR3* fusions have also been reported in breast, biliary, and prostate cancers (5, 6).

Preclinical studies have shown that *FGFR* alterations predict sensitivity to FGFR inhibitors (7, 8). Multiple clinical trials to evaluate FGFR inhibitors, both selective and nonselective, are currently in progress. A phase II trial of dovitinib (TKI258), an FGFR1, FGFR2, and FGFR3 inhibitor, showed activity in estrogen receptor–positive ($ER^+$), FGFR1-amplified breast cancers (9). However, second-line treatment of dovitinib in FGFR2-mutated advanced endometrial cancers did not show any significant activity (10). Lucitanib, an oral, FGFR1/2/3 and VEGFR inhibitor, has shown activity in FGFR1 and FGF3/4/19-amplified tumors (11). Also, JNJ-42756493, an oral pan-FGFR inhibitor, showed significant activity in advanced tumors with FGFR alterations in a phase I dose escalation study (12). As studies with other small-molecule inhibitors have illustrated, despite initial response rates, tumor cells acquire resistance mechanisms with chronic exposure. Therefore, it is important to be cognizant of emerging resistance with treatment. Although *FGFR* alterations appear to predict sensitivity to matching inhibitors, little is known about acquired resistance mechanisms to FGFR inhibition. Consequently, we sought to

[1]Comprehensive Cancer Center, The Ohio State University, Columbus, Ohio. [2]Division of Medical Oncology, Department of Internal Medicine, The Ohio State University, Columbus, Ohio. [3]Center for Biostatistics, Department of Biomedical Informatics, The Ohio State University, Columbus, Ohio. [4]Department of Pharmacology, The Ohio State University, Columbus, Ohio.

**Note:** Supplementary data for this article are available at Molecular Cancer Therapeutics Online (http://mct.aacrjournals.org/).

J. Datta and S. Damodaran contributed equally to this article.

Current address for S. Damodaran: Departments of Breast Medical Oncology and Investigational Cancer Therapeutics, UT MD Anderson Cancer Center, Houston, TX.

**Corresponding Author:** Sameek Roychowdhury, The Ohio State University Comprehensive Cancer Center, 460 West 12th Avenue, Columbus, OH 43210. Phone: 614-685-5842; Fax: 614-292-6356; E-mail: sameek.roychowdhury@osumc.edu

**doi:** 10.1158/1535-7163.MCT-15-1010

Published OnlineFirst March 2, 2017; DOI: 10.1158/1535-7163.MCT-15-1010



identify mechanisms of acquired resistance to FGFR inhibitors utilizing a high-throughput proteomic approach. In this article, we characterize Akt pathway activation in annotated cancer cell lines with activating FGFR alterations as a mechanism of acquired resistance to BGJ398, a selective, oral, pan-FGFR inhibitor.

## Materials and Methods

### Cell lines, reagents, and antibodies

Human cancer cell lines DMS114 (small-cell lung cancer; *FGFR1* amplification) and RT112 (bladder cancer; *FGFR3* fusion and amplification) were obtained from ATCC and CLS, respectively, during December 2012. All the cell lines (control and resistant) were authenticated at the University of Arizona Genetic Core facility (STR profiling) in February 2016. BGJ398 was purchased from Selleck Chemicals. Akt inhibitor, GSK2141795, was purchased from MedChem Express. Inhibitors were prepared as 10 mmol/L stock solutions in DMSO. CellTiter-Glo reagent was purchased from Promega Corporation. Lipofectamine 2000 was obtained from Invitrogen. Control and Akt siRNA were obtained from Cell Signaling Technology. Antibodies to phospho-FRS2α (y196), FGFR1, GSK3α, GSK3β, p-GSK3 α/β S9/S21, p-GSK3 β S9, p-Akt S473, p-Akt T308, pan-Akt, pMEK1/2, MEK1/2, pERK1/2, ERK1/2, pYAP-S127, YAP, TSC1, Cyclin B1, and FOXM1 antibodies were obtained from Cell Signaling Technology. Antibodies against FGFR3, FRS2α, and GAPDH were obtained from Santa Cruz Biotechnology. Antibodies to p-FGFR1 (y653/y654) from EMD Millipore and p-FGFR3 (y724) from Abcam were also utilized.

### Cell culture

DMS114 cell line was cultured in Waymouth's medium supplemented with 10% heat-inactivated FBS, 1% penicillin (100 U/mL), and streptomycin (100 μg/mL). Similarly, RT112 cells were grown in RPMI1640 and 2 mmol/L L-glutamine. Cells were grown as monolayer cultures and maintained in a humidified atmosphere of 5% $CO_2$ in air at 37°C. Cell morphology was monitored using an EVOS XL Core Cell Imaging System under a phase-contrast microscope (Life Technologies). Cells were routinely tested for mycoplasma contamination monthly using the MycoAlert Plus Mycoplasma Detection Kit (Lonza) following the manufacturer's protocol. Cells were last tested in May 2016.

### Cell viability and generation of resistance

Cell lines were treated chronically at a fixed concentration (DMS114; 3 μmol/L) or gradually at increasing concentrations (RT112) with BGJ398. Control cells were treated with vehicle DMSO. To assess the development of resistance, cell cultures were sampled every 4 to 6 weeks and assayed for viability with the CellTiter-Glo assay (Promega). For viability assays, cells were seeded (in quadruplicates) in 96-well plates at a density of 2,000 to 3,000 cells per well in a volume of 100 μL. Twenty-four hours later, media containing BGJ398 or GSK2141795 at various dilutions or DMSO were added. After 72 hours, CellTiter-Glo reagent was added and luminescence was measured following the manufacturer's protocol. Cell viability was evaluated as percentage relative to vehicle controls (100%). Viability curves were plotted using GraphPad Prism software. Upon manifesting resistance, cell lines were maintained with continued drug exposure at concentrations that displayed resistance.

### Western blots

For immunoblots, cell lysates were isolated and homogenized in RIPA buffer (10 mmol/L Tris-HCl, pH 7.5, 150 mmol/L NaCl, 5 mmol/L EDTA, 0.5% SDS, 1.0% NP40, 1.0% sodium deoxycholate, containing protease and phosphatase inhibitors). Total cellular protein was prepared, mixed with 4× Laemmli's buffer, boiled at 97°C for 5 minutes, and then separated on SDS-polyacrylamide gels. Proteins were transferred onto nitrocellulose membranes and probed with antibodies described above. After overnight incubation at 4°C, membranes were blotted for one hour with HRP-conjugated secondary anti-rabbit/mouse antibodies (1:2,500). Next, bound antibody complexes were detected and visualized using enhanced chemiluminescence substrate detection system (Bio-Rad). Blots were stripped and reprobed with GAPDH antibody to control for loading. The intensity of the protein bands was quantified by ImageJ software (https://imagej.nih.gov/ij/).

### Reverse-phase protein array

Control and resistant cell lines were plated in 60-mm culture plates. After 24 hours, cells were lysed using lysis buffer (1% Triton X-100, 50 mmol/L HEPES pH 7.4, 150 nmol/L NaCl, 1.5 mmol/L $MgCl_2$, 1 mmol/L EGTA, 100 mmol/L sodium pyrophosphate, 1 mmol/L $Na_3VO_4$, 10% glycerol, phosphatase and protease inhibitors) and centrifuged at 4°C for 10 minutes at 12,700 × *g*. After protein concentrations were quantified, the lysate was mixed with 4× SDS sample buffer (40% glycerol, 8% SDS, 0.25 mol/L Tris-HCl pH 6.8), boiled for 5 minutes, and stored at −80°C. Subsequently, samples were sent to the Functional Proteomics Core Facility at MD Anderson for reverse-phase protein array (RPPA) analysis.

Briefly, cellular proteins were denatured by 1% SDS (with β-mercaptoethanol) and diluted in five 2-fold serial dilutions (from undiluted to 1:16 dilution) in dilution buffer (lysis buffer containing 1% SDS). Serial diluted lysates were arrayed on nitrocellulose-coated slides (Grace Bio-Labs) by Aushon 2470 Arrayer (Aushon BioSystems). Each slide was probed with a validated primary antibody plus a biotin-conjugated secondary antibody. Only antibodies with a Pearson correlation coefficient between RPPA and Western blotting of greater than 0.7 were used for analysis. The signal obtained was amplified using a DakoCytomation Catalyzed Signal Amplification System (Dako) and visualized by diaminobenzidine colorimetric reaction. The slides were scanned, analyzed, and quantified using a customized software MicroVigene (VigeneTech Inc.) to generate spot intensity. Spots from TIFF images were identified, and the density was quantified by Array-Pro Analyzer software. Each dilution curve was fitted with a logistic model (supercurve fitting) developed by the Department of Bioinformatics and Computational Biology in MD Anderson Cancer Center (Houston, TX). All the data points were normalized for protein loading and transformed to linear values for analysis.

### RNA sequencing

We used 4 μg of each cell line's total RNA and prepared the libraries following Illumina's TruSeq Stranded mRNA Sample Preparation HS (high sample) protocol without modification. We performed 15 cycles of PCR for amplification of the adapter-ligated DNA library and assessed the quality of the final DNA library using the High Sensitivity D1K ScreenTape (TapeStation

Published OnlineFirst March 2, 2017; DOI: 10.1158/1535-7163.MCT-15-1010



2200; Agilent Technologies). Per manufacturer's protocol, library peak size was approximately at 260 bp. We prepared indexed libraries and sent them for 100-bp paired-end sequencing (2 × 100 bp) on an Illumina HiSeq 2000 at Beijing Genomics Institute (China). All four (DMS114, RT112 controls and respective resistant cells) libraries were pooled and sequenced in one lane. Geo accession number is GSE92651.

### RNAi assay

Resistant DMS114 and RT112 cells were plated for 24 hours and were transfected with control or Akt-siRNA targeting Akt1 and Akt2 (60–100 nmol/L) using lipofectamine 2000 following the manufacturer's protocol (Invitrogen). Cells were harvested after 48 hours for protein immunoblot analysis, colony formation, and invasion assays.

### Clonogenic survival assay

Clonogenic survival assay was performed as described previously with minor modifications (13). Briefly, equal number of control siRNA- or Akt siRNA–treated cells were allowed to grow in complete growth media on 60-mm culture plates until visible colonies were formed (12–14 days). Next, cell colonies were rinsed with PBS, fixed with 4% paraformaldehyde, stained with crystal violet solution, washed with water, and air-dried. Visible colonies were counted manually.

### Cell proliferation assay

For cell proliferation assay, resistant cell lines plated on 96 strip–well plate were transfected as described above. Cell viability was monitored every 24 hours for 5 days using the CellTiter-Glo assay. Ratios of cell viability for each day relative to day 1 (24 hours after transfection) were plotted.

### Cell motility assay

Cell motility assays were carried out with the resistant cells transfected in 6-well culture plates (14). After 24 hours of transfection, at approximately 90% confluence, cells were washed with PBS and a fine scratch in the form of a groove was made with the help of a sterile pipette tip and immediately photographed (time 0 hour). Next, cells were supplemented with complete growth medium and allowed to grow. Migration of cells from the edge of the groove toward the center was monitored at 24 hours (×100 magnification). The width of the scratch was measured at 0 hour and at 24 hours to calculate the percentage of the gap covered by the cells in a 24-hour time period.

### Transwell invasion assay

DMS114 and RT112 resistant cells were treated with control and Akt-specific siRNA as described above. Matrigel invasion assay was performed as described previously (15). Briefly, 48 hours after transfection, equal number of control and Akt siRNA–treated resistant cells (30,000) were seeded per well in the Matrigel invasion chambers (Becton Dickinson) and allowed to invade toward 10% FBS containing media (in the bottom of the well). Following incubation of the plate for 24 hours, the noninvaded cells were removed, and the invaded cells at the bottom of the chambers were fixed, stained with violet, washed, and then counted using an inverted microscope (×100 magnification).

### RNA sequencing analysis

To calculate gene expression, TopHat2 (version 2.0.10) was used for aligning the FASTQ files to the human reference genome UCSC build hg19 assembly (16). A UCSC gene annotation file in GTF format was also used during the alignment. The aligned BAM file from TopHat2 was fed into RNASeqQC (version 1.1.7; https://www.broadinstitute.org/cancer/cga/rnaseqc_download) to generate alignment metrics. Gene expression for known genes was calculated as FPKM (fragments per kilobase per million mapped reads) using CuffLinks (version 2.1.1) from the Tuxedo suite, whereas the differentially significant genes from a parent and resistant cell line comparison were found using Cuffdiff (version 2.1.1; ref. 17). The gene annotation file from UCSC was provided to keep the gene format consistent throughout the pipeline.

### Statistical analysis

Descriptive statistics (mean, SD) were used to describe parental and resistant cell lines in viability curves. To compare differences in protein phosphorylation between the parent and resistant cell lines in RPPA, two-sample $t$ test (with equal variances) was utilized. To adjust $P$ values for multiple comparisons, FDR using the Benjamini–Hochberg method was employed (18). A cutoff of FDR <0.05 (q value) was used as a threshold for statistical significance. Microsoft Excel and R (www.r-project.org; v 2.5.0) were used for FDR analysis.

Principal component analysis (PCA) was used to explore the structure of the samples based on protein profiling data in RPPA (19). The samples were projected onto the principle components (i.e., PC1, PC2) for each sample, where PC1 and PC2 are the first two dimensions with the largest variation in the expression data and are the linear combinations of all proteins' expression. Top proteins with largest factor loadings on PC1 and PC2 are identified. Protein expression heatmaps with the imposed two-way hierarchical clustering (based on average linkage and Euclidean distance) were generated for each cell line separately. Heatmaps were generated using MeV 4.9. Statistical analyses for PCA were performed in R 3.2.

## Results

### BGJ398 inhibits FGFR signaling pathway

We assessed the levels of FGFR 1 and 3 in DMS114 and RT112 cell lines by RNA sequencing (RNA-Seq) analysis (Supplementary Table S1). Western blot analysis confirmed that RT112 has FGFR3 expression and no FGFR1, whereas DMS114 has mainly FGFR1 with a small amount of FGFR3 expression (Supplementary Fig. S1). Next, we assessed the effect of BGJ398 on total and phosphorylated forms of FGFR (FGFR1 for DMS114 and FGFR3 for RT112) and its substrate FRS2 (Fig. 1). Western blots showed dose-dependent decreases in phosphorylation of FGFR and FRS2 in both the cell lines, demonstrating that BGJ398 (Supplementary Fig. S2) inhibits FGFR signaling. The levels of total FGFR1/FGFR3 and FRS2 were also significantly decreased in a dose-dependent manner. On the other hand, Total MEK and ERK were not affected even at higher doses indicating FGFR specificity (Fig. 1).

### Development of resistance to BGJ398

We cultured DMS114 and RT112 cell lines, in the presence of DMSO (vehicle control) or BGJ398 at fixed concentration or gradually increasing concentrations, chronically to stimulate acquired resistance. With prolonged exposure, both resistant cell

Published OnlineFirst March 2, 2017; DOI: 10.1158/1535-7163.MCT-15-1010



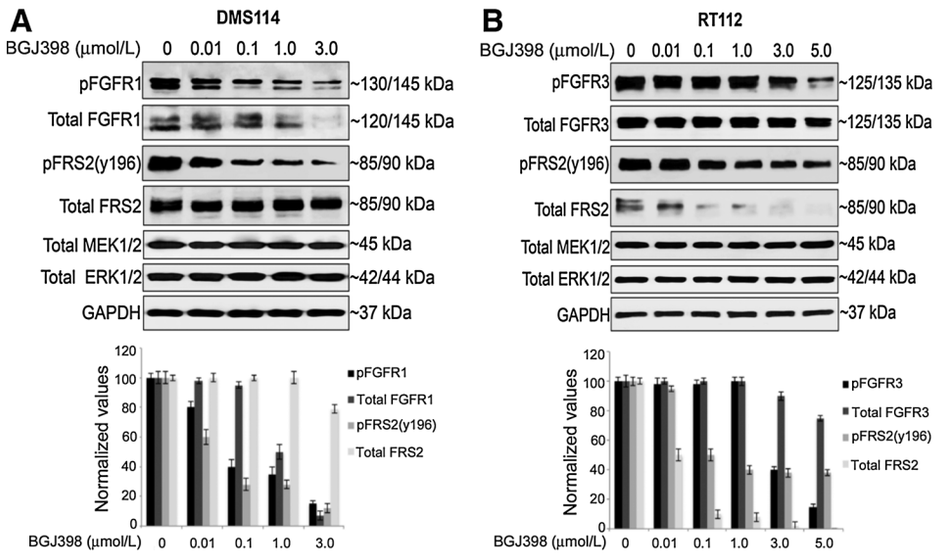


**Figure 1.**
BGJ398 inhibits signaling in cell lines with activating FGFR alterations. Immunoblot demonstrates the expression of total/pFGFRs and total/pFRS2 in DMSO and BGJ398 in treated cell lines (**A**) DMS114. **B,** RT112. Lysates were prepared from cells exposed to BGJ398 (at the indicated concentrations) for 24 hours and immunoblots performed with the respective antibodies. Representative data are shown from three experimental replicates. Bar graphs display densitometric analysis of protein bands using GAPDH as a control. BGJ398 treatment results in decreased levels of pFGFR1/pFGFR3 and pFRS2/total FRS2, respectively.

lines displayed marked differences in the sensitivity to BGJ398 compared with the corresponding controls (Fig. 2A). Morphologically, resistant cell lines were irregular, elongated with protrusions, whereas the control cells were regular and remained in clusters, as described previously (Supplementary Fig. S3; ref. 20). Next, we performed Western blots to evaluate the total and phosphorylated forms of FGFR1/FGFR3 (DMS114/RT112) and FRS2 in the control and resistant cell lines. We observed significant decreases in pFGFR1 or 3, total FGFR1 or 3, and pFRS2 in DMS114 and RT112 cell lines compared with controls (Fig. 2B) However, there was no significant change in total FRS2. Western blotting data corroborated that BGJ398 continued to block FGFR activity in both the resistant cell lines (Fig. 2B) without any appreciable effect on cell viability (Fig. 2A).

### RPPA demonstrates Akt activation in BGJ398-resistant cell lines

To identify differentially phosphorylated proteins in the BGJ398-resistant cells, we performed RPPA analysis for both resistant cell lines and their respective DMSO-treated controls. Heatmaps showed differential expression of proteins between the resistant and control cell lines (Supplementary Fig. S4; Supplementary Tables S2 and S3). Using FDR <0.05, we identified proteins differentially expressed for each of the resistant cell lines compared with controls (Fig. 3A; Supplementary Tables S4 and S5). Next, we investigated protein changes that were common in both DMS114 and RT112 resistant cell lines (differentially up- or downregulated). Increased levels of pAkt (T308 and S473), pGSK3β (S9), and pGSK3α/β (S21/S9) were observed in resistant cell lines compared with the controls (Fig. 3B). However, the levels of phosphorylation significantly varied between the two cell lines, with DMS114 showing markedly higher levels of Akt and GSK3 phosphorylation compared with the RT112 cell line (Table 1). Phosphorylated YAP (pYAP-S127) and TSC1 levels were also significantly higher in the resistant lines compared with their respective controls (Table 1). Conversely, Cyclin B1 and FOXM1 were downregulated in the resistant cell lines. PCA revealed that the resistant cell lines clustered separately from their corresponding control cell lines (Supplementary Fig. S5). Factor-loading plots for each principal component (PC) were created to identify the proteins responsible for group clustering. Data for all proteins in RPPA were projected in the first two dimensions (PC1 and PC2). As PC1 seemed to best associate with group clustering, the top 20 proteins for PC1 were determined (Supplementary Fig. S5). PCA showed Akt phosphorylation (S473 and T308) as PC1 in both the resistant cell lines.

### Validation of RPPA protein changes by Western blot analysis

Next, we performed Western blots to corroborate pAkt (S473, T308), pGSK3β (S9), pGSK3α/β (S21/S9), pYAP (S127), and TSC1 proteins that were upregulated in resistant cell lines compared with the controls. These were performed with the same protein extracts used for RPPA. There were increased levels of phosphorylation of Akt (both S473 and T308), pGSK3β (S9), and pGSK3α/β (S21/S9) observed in both the resistant cell lines compared with their matching control cell lines (Fig. 3C). Although there were no appreciable changes in total levels of these proteins in DMS114, lower levels of total Akt were observed in resistant RT112 cells. Furthermore, phosphorylated YAP (S127) and TSC1 protein expression were significantly higher compared with the corresponding controls. These changes were concordant with the changes that were observed in RPPA (Table 1; Fig. 3; Supplementary Tables S4 and S5). In contrast, Western blot data demonstrated upregulation of Cyclin B1 and FOXM1 (Fig. 3C) in the resistant cell lines. Furthermore, decreases in phosphorylation of MEK and ERK were observed in resistant DMS114 and RT112 cells (Supplementary Fig. S6). Taken together, data from RPPA and Western blots demonstrated Akt pathway activation in both the resistant FGFR cell lines as evidenced by increased phosphorylation of Akt and its downstream substrate GSK3. We reviewed RPPA data to identify upstream RTKs that could potentially activate Akt. No significant changes in ERBB2, EGFR, and MET were observed in DMS114-R (Supplementary Table S4). On the other hand, lower levels of EGFR and ERBB2 were observed in RT112-R (Supplementary Table S5). However, RNA-Seq analysis did not reveal any significant changes in the expression of EGFR, ERBB2, or MET (Supplementary Table S6). Although RNA-Seq showed increased EGFR expression in DMS114-R, this was not statistically significant ($q = 0.91$).

Published OnlineFirst March 2, 2017; DOI: 10.1158/1535-7163.MCT-15-1010



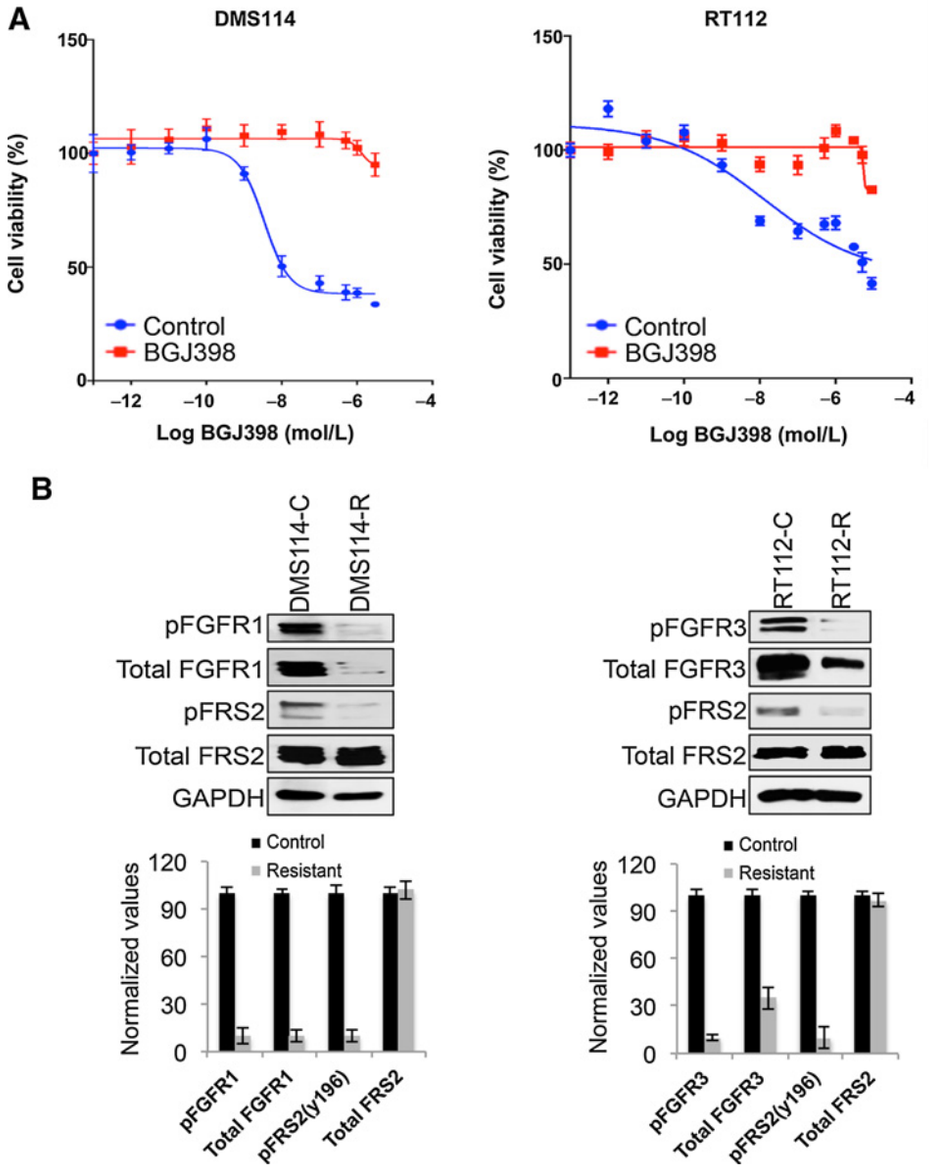


**Figure 2.**
Development of resistance after chronic exposure to BGJ398. **A,** Resistance was induced by chronic exposure of DMS114 and RT112 cell lines to BGJ398. Control cells were treated with DMSO. Panel shows viability curves performed with CellTiter-Glo assay. Control and resistant cells were treated with BGJ398 at different concentrations as indicated, and viable cells were measured after 72 hours. The percentage of viable cells is shown relative to DMSO vehicle-treated controls (mean ± SD). Assays were performed in quadruplicates (three experimental replicates). **B,** Western blot analysis was performed with the lysates from control and resistant cells to assess FGFR signaling as measured by pFGFR1/3 and pFRS2 (three experimental replicates).

**BGJ398-resistant cell lines are sensitive to Akt inhibitor GSK2141795**

As Akt pathway was activated in the resistant lines, we examined whether the addition of an Akt inhibitor, GSK2141795 (Supplementary Fig. S2) could potentially restore sensitivity to BGJ398. Treatment of DMS114-R cell line with GSK2141795 alone resulted in a significant decrease in cell viability with dose as low as 100 nmol/L, although increasing doses reduced cell viability further, with 80% decrease noticed at 3 μmol/L concentration of GSK2141795 (Fig. 4A). Low doses of GSK2141795 had no effect on cell viability in the DMS114 control cell line, whereas a high dose (3 μmol/L) had a mild effect. Although the combination of BGJ398 (100 nmol/L) with GSK2141795 (100 nmol/L) produced a significant reduction in cell viability, this effect was not significant compared with the use of GSK2141795 as a single agent, indicating that treatment of Akt inhibitor alone is sufficient to inhibit the viability of BGJ398-resistant DMS114 cells (Fig. 4A). Thus, Akt signaling pathway is highly activated in the BGJ398-resistant DMS114 cell line, and treatment with GSK2141795 inhibits cell viability. Although the RT112-R cells exhibited sensitivity to GSK2141795 in a dose-dependent manner, the $IC_{50}$ was higher (6 μmol/L). Furthermore, unlike DMS114, the RT112 control cells showed some sensitivity to GSK2141795 albeit lower than RT112-R (Fig. 4A). In addition, combination treatment of GSK2141795 and BGJ398 did not have any additive effect on RT112-R. The disparities in sensitivity to GSK2141795 is presumably due to differences in the level of activation and dependence on Akt pathway between the resistant cell lines [there was nearly a 30-fold increase in Akt (S473) phosphorylation in DMS114-R compared with RT112-R; Table 1; Supplementary Table S7]. We performed Western blots to corroborate that GSK2141795 affects cell viability in resistant FGFR cell lines through its inhibitory effect on the Akt pathway (Fig. 4B). Resistant lines demonstrated significantly reduced phosphorylation of

Published OnlineFirst March 2, 2017; DOI: 10.1158/1535-7163.MCT-15-1010



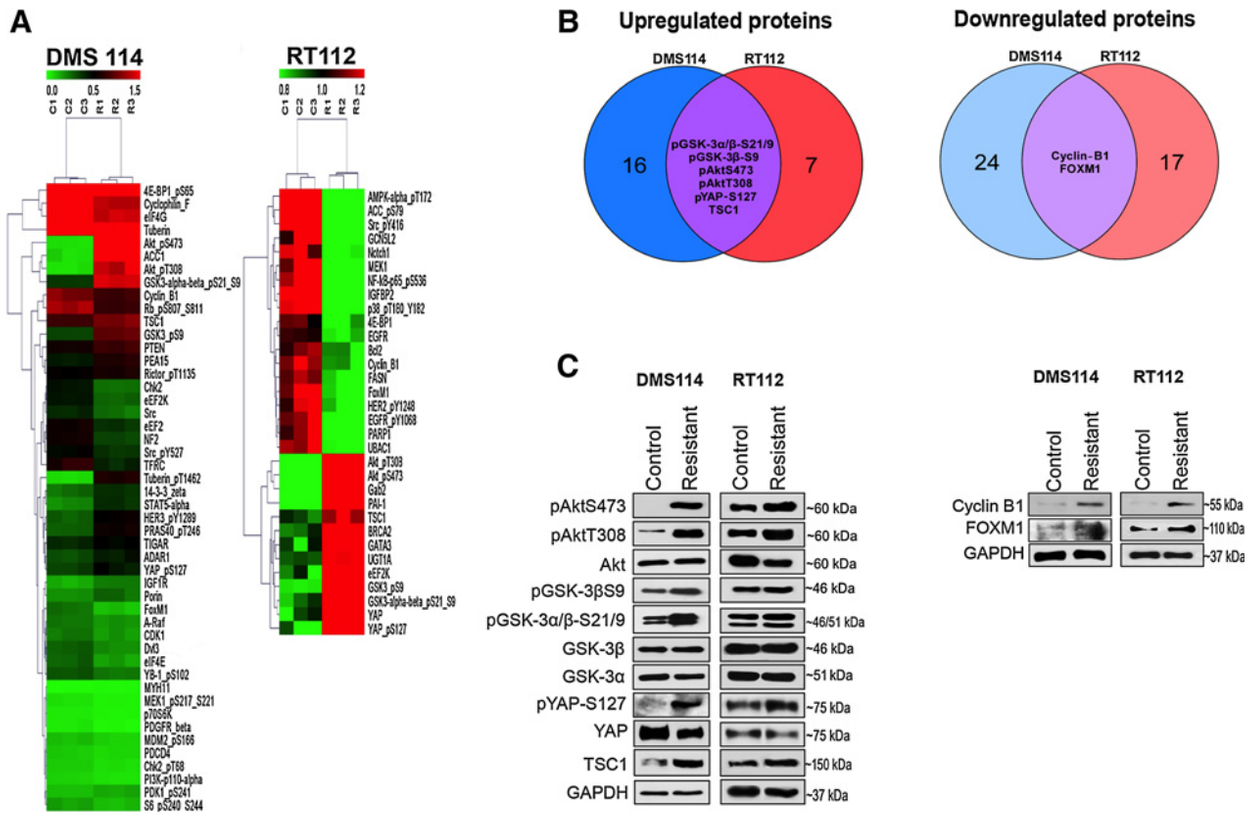


**Figure 3.**

RPPA reveals Akt pathway activation in BGJ398-resistant cell lines. **A,** Heatmaps show RPPA proteins that were differentially phosphorylated in resistant and control ($q < 0.05$) DMS114 and RT112 cell lines. **B,** Venn diagram shows proteins that were commonly upregulated (left) and downregulated (right) in both resistant cell lines **C.** Western blot analysis to confirm protein changes that were upregulated (left) and downregulated (3) in resistant cell lines (representative data from three experimental replicates are shown).

GSK3β (S9) and GSK3α/β (S21/S9), the downstream targets of Akt. Interestingly, increased phosphorylation of Akt (S473 and T308) was observed in both the resistant cell lines with GSK2141795 treatment, likely due to feedback increase in Akt phosphorylation as described previously (21, 22). Overall, these results suggest that Akt pathway activation can mediate acquired resistance to FGFR targeting, and Akt inhibitor treatment can restore sensitivity.

### siRNA-mediated Akt knockdown inhibits growth and migration of resistant FGFR cancer cells

RNA-Seq analysis showed that Akt1 and Akt2 are the commonest isoforms in DMS114 and RT112 cell lines (Supplementary Table S7). Next, we used an Akt siRNA that specifically inhibited Akt1 and Akt2 expression. We evaluated the effect of siRNA treatment on the levels of Akt phosphorylation and its downstream substrates, GSK3β and GSK3α/β. Treatment of

**Table 1.** Protein changes in resistant FGFR cell lines

| Cell line | Protein | Percent change (up/down) | *P* | q-value |
|---|---|---|---|---|
| DMS114 | Akt_pS473 | 3622.68645 | 1.54E−06 | 0.00016487 |
| | Akt_pT308 | 2252.07737 | 6.47E−05 | 0.00125812 |
| | GSK3-alpha-beta_pS21_S9 | 284.091792 | 2.50E−07 | 5.35E−05 |
| | GSK3_pS9 | 187.53704 | 4.94E−06 | 0.00026516 |
| | YAP_pS127 | 32.06119 | 0.01389659 | 0.04373338 |
| | TSC1 | 31.3146193 | 0.00084919 | 0.00586215 |
| | Cyclin_B1 | −24.410473 | 0.00499741 | 0.02088713 |
| | FoxM1 | −56.218837 | 0.00027636 | 0.00295707 |
| RT112 | Akt_pS473 | 123.622596 | 0.00038911 | 0.01055472 |
| | Akt_pT308 | 203.350928 | 0.00126369 | 0.01890811 |
| | GSK3-alpha-beta_pS21_S9 | 41.1993588 | 0.00134332 | 0.01890811 |
| | GSK3_pS9 | 64.2870708 | 0.00011599 | 0.00629257 |
| | YAP_pS127 | 76.7742588 | 0.00493268 | 0.04129296 |
| | TSC1 | 24.6593776 | 0.0027762 | 0.02868744 |
| | Cyclin_B1 | −28.205219 | 0.0065222 | 0.04424411 |
| | FoxM1 | −36.057898 | 0.0022811 | 0.0261498 |

Published OnlineFirst March 2, 2017; DOI: 10.1158/1535-7163.MCT-15-1010



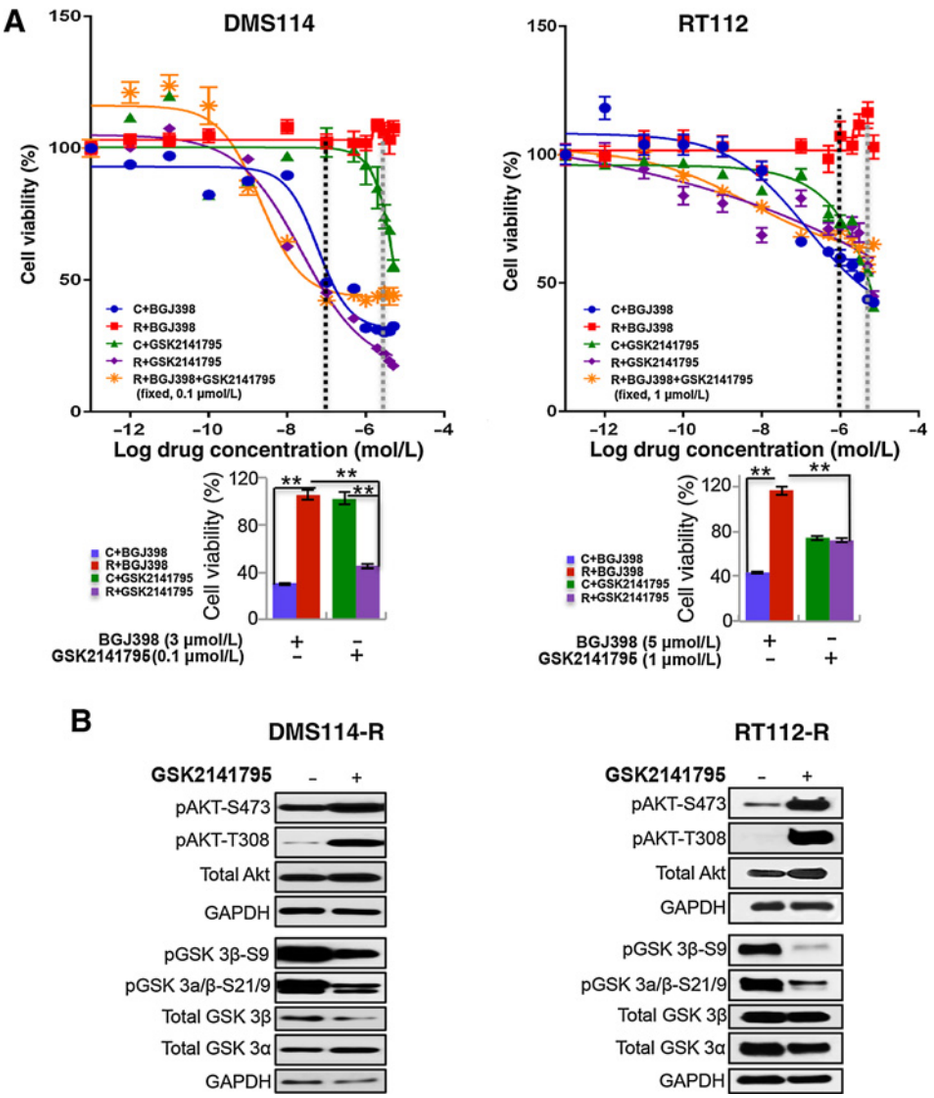


**Figure 4.**
BGJ398-resistant cell lines are sensitive to Akt inhibitor. **A,** Viability curves for control and resistant cells treated with DMSO vehicle, BGJ398 (varying concentrations as indicated), and GSK2141795 (at a fixed concentration: DMS114 0.1, μmol/L; RT112, 1 μmol/L) for 72 hours. Gray and black vertical dotted lines denote 3 μmol/L and 0.1 μmol/L (DMS114), 5 μmol/L and 1 μmol/L (RT112) drug concentrations, respectively, that are shown in the bar graph below. Bar graphs show differences in cell viability in control and resistant cell lines to BGJ398 and GSK2141795. Assays performed in quadruplicates and data are presented as mean ± SD (three experimental replicates). **, Statistical significant difference, $P < 0.001$. **B,** Western blot analysis was performed with lysates from resistant cell lines treated either with vehicle (DMSO) or GSK2141795 (1 μmol/L) for 24 hours to assess inhibition of Akt (pAKT) and downstream (pGSK3) signaling (three experimental replicates).

each resistant cell line with Akt siRNA resulted in significant decreases in both the total Akt and pAkt (S473 and T308) expression compared with their respective siRNA control–treated cells ($P < 0.001$; Fig. 5A). Differential levels of total Akt depletion was observed in DMS114-R (~80%) and RT112-R (~70%) cell lines. This could potentially be due to variation in transfection efficiency between these cell lines. No effect was observed on MEK1/2 phosphorylation, confirming the specificity of Akt siRNA. Although the levels of both total GSK3α/β and their phosphorylated forms (S21/S9) were decreased significantly with Akt siRNA–treated DMS114-R, the levels of pGSK3α/β (S21/S9) were only moderately decreased with Akt siRNA in RT112-R compared with control siRNA cells. Furthermore, we tested whether Akt siRNA treatment affected cell proliferation, colony formation, cell migration, and cell invasion in resistant lines (Fig. 5B–D). Cell proliferation was reduced in resistant cell lines following Akt siRNA treatment. Consistent with Akt inhibitor treatment, the observed effect of siRNA was lower in RT112-R in comparison with DMS114-R cell line. Akt siRNA treatment also significantly inhibited colony formation, cell migration, and cell invasion in both resistant cell lines compared with controls (Fig. 5C and D, $P < 0.001$).

## Discussion

Activation of FGFR signaling pathway due to *FGFR* gene amplifications, mutations, or fusions has been identified in various cancers, such as, lung, bladder, biliary, and breast (1). While therapeutic strategies targeting FGFR are being explored in clinical trials, we sought to study acquired drug resistance in annotated cancer cell lines (23–25). As observed with inhibition of other oncogenic kinases, such as ALK and BRAF, we hypothesized that oncogenic addiction could lead to reactivation of downstream elements of FGFR signaling (26, 27). Also, secondary resistance can be mediated due to clonal selection of resistant cells, often present prior to treatment, with observed clonal divergence across various metastatic sites (28, 29). We applied

Published OnlineFirst March 2, 2017; DOI: 10.1158/1535-7163.MCT-15-1010



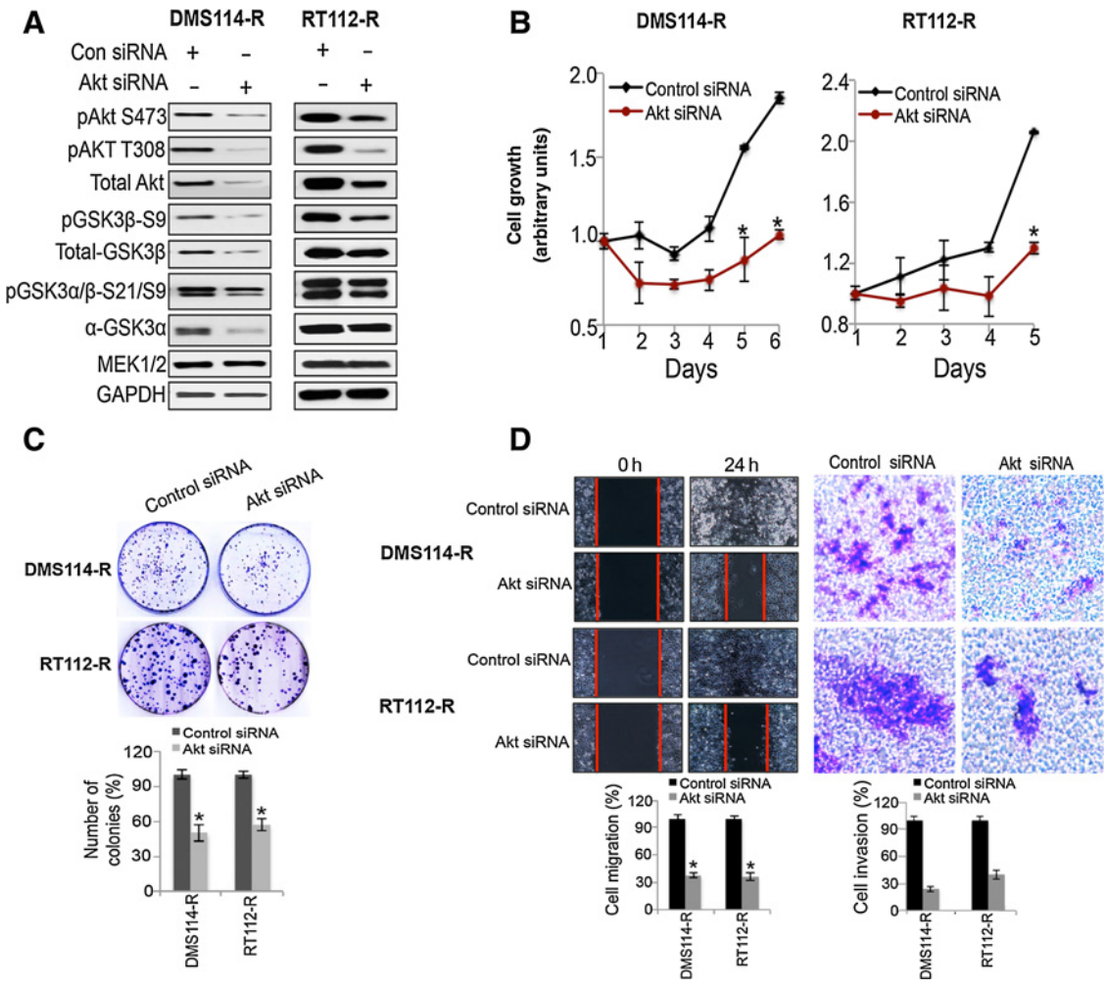


**Figure 5.**

BGJ398-resistant cell lines are sensitive to Akt siRNA knockdown. **A,** Resistant cells were treated with control siRNA or Akt siRNA (60 nmol/L for 48 hours). Whole-cell protein lysates were extracted, and immunoblots were performed to assess Akt and downstream proteins. Representative data have been shown (three experimental replicates). **B,** Resistant cells were transfected with control or Akt-specific siRNA, and cell proliferation was measured using the CellTiter-Glo assay (mean ± SD; *, $P < 0.005$). Assays were performed in quadruplicates with four experimental replicates. **C,** Colonies were stained with crystal violet and counted after transfection (control or Akt siRNA) of resistant cell lines. Bar graph shows colony counts in control and Akt siRNA–treated resistant cell lines (mean ± SD; *, $P \leq 0.005$). Each assay was performed in triplicate with three experimental replicates. **D,** Left, motility assay was performed after treatment with control or Akt siRNA (magnification, ×100). Bar graphs depict the surface area covered by the cells at 24 hours (mean ± SD; *, $P \leq 0.005$). Right, invasion assay was performed using Boyden chamber after treatment with control or Akt siRNA. Bar graphs depict the number of cells that migrated through the Matrigel at 24 hours (mean ± SD; *, $P \leq 0.005$). Representative data from three experimental replicates are shown.

a high-throughput proteomics approach to identify candidates for acquired resistance. Early preclinical work may guide evaluation of precious clinical tumor specimens from patients participating in ongoing therapeutic trials.

In this study, we generated two cell lines, DMS114 (small-cell lung cancer line with *FGFR1* amplification) and RT112 (bladder carcinoma with *FGFR3-TACC3* fusion and *FGFR3* amplification) as manifesting acquired resistance after chronic BGJ398 exposure, based on viability assays (Fig. 2). To assess the relative activity of proteins involved in FGFR signal transduction, we performed proteomic analysis with RPPA. RPPA demonstrated Akt pathway activation in both the resistant cell lines despite ongoing FGFR blockade in the presence of BGJ398 (Fig. 3). These results were corroborated with Western blots. Treatment of the resistant cells with Akt siRNA or GSK2141795, an oral, competitive, pan-isoform Akt inhibitor, currently under evaluation in clinical trials (30, 31), was able to restore sensitivity of resistant cell lines (Figs. 4 and 5).

Activated FGFR signals primarily through one of three pathways: MAPK, PI3K/Akt/mTOR, and phospholipase C-gamma (PLCγ). FGFR preferentially signals through FRS2 to the MAPK pathway, although depending on the cellular context, other pathways, such as p38 MAPK and STAT, could also be activated (1). Activated Akt, mediated by phosphorylation at T308 by PDK1 and phosphorylation at S473 by PDK2, regulates multiple downstream substrates, including GSK3 α/β, FOXO, PRAS40, and TSC1/2 (32). Phosphorylation of S9 in GSK3β or S21 in GSK3α mediated by Akt can potentially lead to reactivation of β-catenin,

Published OnlineFirst March 2, 2017; DOI: 10.1158/1535-7163.MCT-15-1010



which in turn can increase cyclin D1 and transcription factor activity leading to cell-cycle progression (33–35). Increased phosphorylation of GSK3α at S21 and GSK3β at S9 was observed in both the resistant cell lines consistent with Akt activation. Furthermore, an increase in phosphorylation of proline-rich Akt substrate of 40 kDa (PRAS40) at T246 was observed in DMS114-R. PRAS40 is a crucial mediator of Akt signaling and its phosphorylation (T246), mediated by Akt, facilitates the binding of 14-3-3 protein, which disrupts the inhibitory action of PRAS40 on mTORC1 leading to phosphorylation of downstream substrates (e.g., S6 kinase, 4EBP1) and cell growth (36, 37). Accordingly, increased expression of 14-3-3 (ζ) was observed in DMS114-R. Overall, data from RPPA substantiated activation of Akt pathway in cell lines resistant to BGJ398.

Several studies have suggested a reciprocal relationship between FGFR and other members of the RTK family in mediating acquired resistance to FGFR inhibition. Herrera-Abreu and colleagues used parallel RNA interference genetic screens to show that EGFR activation limits sensitivity to FGFR inhibition in cell lines with *FGFR3* mutations (38). Conversely, activation of FGF2–FGFR1 pathway has been shown to mediate acquired resistance to EGFR inhibition in lung cancer (39). Ligand-mediated activation of ERBB2/3 was shown to mediate resistance to FGFR3 inhibition (40). Similarly, HGF-mediated ligand activation of MET was shown to rescue RT112 cells from the effect of FGFR inhibition by BGJ398, suggesting that compensatory activation of other members of the RTK family can mediate resistance to FGFR targeting (41). In contrast, Chell and colleagues identified a secondary gatekeeper mutation in FGFR3 (V555M) as a mechanism of acquired resistance to ATP-competitive FGFR inhibitors, AZD4547 and PD173074 (42). In our study, despite differences in the tissue of origin and the genomic alteration in FGFR, the resistant cell lines showed activation of Akt pathway, suggesting secondary activation of bypass signaling as a potential mechanism of resistance to FGFR targeting.

Our observation is consistent with what has been previously described with respect to a prominent role for Akt in FGFR signaling (43). Hu and colleagues observed that FGFR inhibition with BGJ398 led to transient inhibition of ERK1/2 phosphorylation due to negative feedback, whereas the effect on Akt phosphorylation was sustained in RT112 and KATOIII cell lines. In addition, they showed that a constitutively activated form of Akt (myristoylated Akt) effectively rescued cells from BGJ398 growth inhibition. Grygielewicz and colleagues evaluated resistance in SNU-16, an *FGFR2*-amplified gastric cancer cell line, to FGFR inhibitors AZD4547, BGJ398, and PD173074. While epithelial–mesenchymal transition was primarily implicated as mediating resistance to the FGFR inhibitors, increased levels of pAkt (along with pSTAT and pERK) were observed in the resistant cell lines and treatment with pictilisib, a PI3K inhibitor, was able to restore sensitivity (44). Furthermore, acquired resistance to cetuximab, an mAb for EGFR, was associated with Akt activation in lung cancer cell lines, and pharmacologic inhibition of Akt with the PI3K inhibitor LY294002 enhanced the inhibitory effect of cetuximab (45). Thus, there is interest in whether Akt or PI3K inhibitors could overcome resistance in cancers driven by RTKs. Although there is a breadth of candidate mechanisms of resistance in preclinical models suggesting a potential role for combination therapies with FGFR inhibitors, this will depend on the evaluation of resistance in patient tumor samples in ongoing clinical trials.

To characterize resistance mechanisms in patients, pretreatment and postprogression tumor biopsies will be needed to support assays such as RPPA, DNA/RNA-Seq, or patient-derived xenograft studies. However, tumor specimens are finite and may not be able to practically support all of these assays. Consequently, preclinical models are often utilized to provide preliminary evidence of resistance mechanisms in humans and guide evaluation in precious tumor specimens. In addition to tumor biopsies, circulating tumor cells or circulating tumor DNA (ctDNA) may provide a rapid and noninvasive strategy to assess resistance in cases where tumors cannot be readily biopsied. For example, using ctDNA and xenograft, secondary NTRK1 mutations were identified as a resistance mechanism to entrectinib, a pan-TRK inhibitor, in an advanced colorectal cancer patient with an *NTRK1* fusion (46). Similarly, ctDNA has been successfully utilized to track clonal evolution and resistance to EGFR inhibition (47). Identification of resistance mechanisms can potentially reveal rational targeted therapy combinations. The understanding that reactivation of MAPK pathway mediates resistance to BRAF inhibition led to the use of combination of BRAF and MEK inhibitors in melanoma patients harboring BRAF V600 mutations, leading to improved survival (48). In another example, identification of PI3K/Akt/mTOR pathway activation as a mechanism of resistance to endocrine therapy led to the evaluation and approval of combination of everolimus, an mTOR inhibitor, and exemestane in hormone receptor–positive breast cancer patients (49). Our study provides preclinical evidence that activation of Akt mediates resistance to FGFR inhibition, supports the need for further evaluation of this pathway in patients, and underscores a potential opportunity for combination therapy.

## Disclosure of Potential Conflicts of Interest

S. Roychowdhury receives funding from Novartis and Ariad Pharmaceuticals for conducting clinical trials. S.Roychowdhury's immediate family members own stock in Johnson and Johnson. No potential conflicts of interest were disclosed by the other authors.

## Authors' Contributions

**Conception and design:** S. Damodaran, J. Datta, H. Parks, J. Hays, S. Roychowdhury

**Development of methodology:** S. Damodaran, J. Datta, H. Parks, J. Hays

**Acquisition of data (provided animals, acquired and managed patients, provided facilities, etc.):** S. Damodaran, J. Datta, C. Ocrainiciuc, E.P. Gardner

**Analysis and interpretation of data (e.g., statistical analysis, biostatistics, computational analysis):** S. Damodaran, J. Datta, H. Parks, C. Ocrainiciuc, J. Miya, L. Yu, E.P. Gardner, E. Samorodnitsky, M.R. Wing, J. Hays

**Writing, review, and/or revision of the manuscript:** S. Damodaran, J. Datta, J. Miya, L. Yu, J. Hays, J.W. Reeser, S. Roychowdhury

**Administrative, technical, or material support (i.e., reporting or organizing data, constructing databases):** J. Datta, D. Bhatt

**Study supervision:** J. Datta, J. Hays, S. Roychowdhury

## Acknowledgments

We would like to acknowledge the Comprehensive Cancer Center (CCC), Arthur G. James Cancer Hospital and Richard A. Solove Research Institute at The Ohio State University Wexner Medical Center, and The Ohio Supercomputer Center for supporting this study. We also would like to thank Esko Kautto and Mikayla Dantuono for technical help and Jenny Badillo for administrative support.

## Grant Support

S. Damodaran was supported by the American Society of Clinical Oncology Young Investigator Award. E. Samorodnitsky was supported by a Pelotonia Postdoctoral Fellowship. S. Roychowdhury was supported by the American

Cancer Society (MRSG-12-194-01-TBG), the Prostate Cancer Foundation, NHGRIUM1HG006508-01A1, Fore Cancer Research, American Lung Association, and Pelotonia.

The costs of publication of this article were defrayed in part by the payment of page charges. This article must therefore be hereby marked *advertisement* in accordance with 18 U.S.C. Section 1734 solely to indicate this fact.

Received December 28, 2015; revised December 21, 2016; accepted December 25, 2016; published OnlineFirst March 2, 2017.

## References

1. Turner N, Grose R. Fibroblast growth factor signalling: from development to cancer. Nat Rev Cancer 2010;10:116–29.
2. Yang F, Zhang Y, Ressler SJ, Ittmann MM, Ayala GE, Dang TD, et al. FGFR1 is essential for prostate cancer progression and metastasis. Cancer Res 2013;73:3716–24.
3. Weiss J, Sos ML, Seidel D, Peifer M, Zander T, Heuckmann JM, et al. Frequent and focal FGFR1 amplification associates with therapeutically tractable FGFR1 dependency in squamous cell lung cancer. Sci Transl Med 2010;2:62ra93.
4. Wesche J, Haglund K, Haugsten EM. Fibroblast growth factors and their receptors in cancer. Biochem J 2011;437:199–213.
5. Williams SV, Hurst CD, Knowles MA. Oncogenic FGFR3 gene fusions in bladder cancer. Hum Mol Genet 2013;22:795–803.
6. Wu YM, Su F, Kalyana-Sundaram S, Khazanov N, Ateeq B, Cao X, et al. Identification of targetable FGFR gene fusions in diverse cancers. Cancer Discov 2013;3:636–47.
7. Guagnano V, Kauffmann A, Wohrle S, Stamm C, Ito M, Barys L, et al. FGFR genetic alterations predict for sensitivity to NVP-BGJ398, a selective pan-FGFR inhibitor. Cancer Discov 2012;2:1118–33.
8. Gozgit JM, Wong MJ, Moran L, Wardwell S, Mohemmad QK, Narasimhan NI, et al. Ponatinib (AP24534), a multitargeted pan-FGFR inhibitor with activity in multiple FGFR-amplified or mutated cancer models. Mol Cancer Ther 2012;11:690–9.
9. Andre F, Bachelot T, Campone M, Dalenc F, Perez-Garcia JM, Hurvitz SA, et al. Targeting FGFR with dovitinib (TKI258): preclinical and clinical data in breast cancer. Clin Cancer Res 2013;19:3693–702.
10. Konecny GE, Finkler N, Garcia AA, Lorusso D, Lee PS, Rocconi RP, et al. Second-line dovitinib (TKI258) in patients with FGFR2-mutated or FGFR2-non-mutated advanced or metastatic endometrial cancer: a non-randomised, open-label, two-group, two-stage, phase 2 study. Lancet Oncol 2015;16:686–94.
11. Soria JC, DeBraud F, Bahleda R, Adamo B, Andre F, Dienstmann R, et al. Phase I/IIa study evaluating the safety, efficacy, pharmacokinetics, and pharmacodynamics of lucitanib in advanced solid tumors. Ann Oncol 2014;25:2244–51.
12. Tabernero J, Bahleda R, Dienstmann R, Infante JR, Mita A, Italiano A, et al. Phase I dose-escalation study of JNJ-42756493, an oral pan-fibroblast growth factor receptor inhibitor, in patients with advanced solid tumors. J Clin Oncol 2015;33:3401–8.
13. Franken NA, Rodermond HM, Stap J, Haveman J, van Bree C. Clonogenic assay of cells *in vitro*. Nat Protoc 2006;1:2315–9.
14. Islam M, Datta J, Lang JC, Teknos TN. Down regulation of RhoC by microRNA-138 results in de-activation of FAK, Src and Erk1/2 signaling pathway in head and neck squamous cell carcinoma. Oral Oncol 2014;50:448–56.
15. Valster A, Tran NL, Nakada M, Berens ME, Chan AY, Symons M. Cell migration and invasion assays. Methods 2005;37:208–15.
16. Kim D, Pertea G, Trapnell C, Pimentel H, Kelley R, Salzberg SL. TopHat2: accurate alignment of transcriptomes in the presence of insertions, deletions and gene fusions. Genome Biol 2013;14:R36.
17. Trapnell C, Williams BA, Pertea G, Mortazavi A, Kwan G, van Baren MJ, et al. Transcript assembly and quantification by RNA-Seq reveals unannotated transcripts and isoform switching during cell differentiation. Nat Biotechnol 2010;28:511–5.
18. Benjamini Y, Hochberg Y. Controlling the false discovery rate: a practical and powerful approach to multiple testing. J Royal Stat Soc Ser B 1995;57:289–300.
19. Abdi H, Williams LJ. Principal component analysis. Wiley Interdiscip Rev Comput Stat 2010;2:433–59.
20. Du F, Wu X, Liu Y, Wang T, Qi X, Mao Y, et al. Acquisition of paclitaxel resistance via PI3Kdependent epithelialmesenchymal transition in A2780 human ovarian cancer cells. Oncol Rep 2013;30:1113–8.
21. Dumble M, Crouthamel MC, Zhang SY, Schaber M, Levy D, Robell K, et al. Discovery of novel AKT inhibitors with enhanced anti-tumor effects in combination with the MEK inhibitor. PLoS One 2014;9:e100880.
22. Rhodes N, Heerding DA, Duckett DR, Eberwein DJ, Knick VB, Lansing TJ, et al. Characterization of an Akt kinase inhibitor with potent pharmacodynamic and antitumor activity. Cancer Res 2008;68:2366–74.
23. Johannessen CM, Boehm JS, Kim SY, Thomas SR, Wardwell L, Johnson LA, et al. COT drives resistance to RAF inhibition through MAP kinase pathway reactivation. Nature 2010;468:968–72.
24. Nazarian R, Shi H, Wang Q, Kong X, Koya RC, Lee H, et al. Melanomas acquire resistance to B-RAF(V600E) inhibition by RTK or N-RAS upregulation. Nature 2010;468:973–7.
25. Poulikakos PI, Persaud Y, Janakiraman M, Kong X, Ng C, Moriceau G, et al. RAF inhibitor resistance is mediated by dimerization of aberrantly spliced BRAF(V600E). Nature 2011;480:387–90.
26. Lito P, Rosen N, Solit DB. Tumor adaptation and resistance to RAF inhibitors. Nat Med 2013;19:1401–9.
27. Wilson FH, Johannessen CM, Piccioni F, Tamayo P, Kim JW, Van Allen EM, et al. A functional landscape of resistance to ALK inhibition in lung cancer. Cancer Cell 2015;27:397–408.
28. Turke AB, Zejnullahu K, Wu YL, Song Y, Dias-Santagata D, Lifshits E, et al. Preexistence and clonal selection of MET amplification in EGFR mutant NSCLC. Cancer Cell 2010;17:77–88.
29. Morrissy AS, Garzia L, Shih DJ, Zuyderduyn S, Huang X, Skowron P, et al. Divergent clonal selection dominates medulloblastoma at recurrence. Nature 2016;529:351–7.
30. ClinicalTrials.gov. Trametinib and Akt inhibitor GSK2141795 in treating patients with metastatic triple-negative breast cancer. Bethesda, MD: NIH; 2017. Available from: https://www.clinicaltrials.gov/ct2/show/NCT01964924.
31. Burris HA, Siu LL, Infante JR, Wheler JJ, Kurkjian C, Opalinska J, Smith DA, et al. Safety, pharmacokinetics (PK), pharmacodynamics (PD), and clinical activity of the oral AKT inhibitor GSK2141795 (GSK795) in a phase I first-in-human study. J Clin Oncol 29: 2011(suppl; abstr 3003).
32. Franke TF. PI3K/Akt: getting it right matters. Oncogene 2008;27:6473–88.
33. Luo J. Glycogen synthase kinase 3beta (GSK3beta) in tumorigenesis and cancer chemotherapy. Cancer Lett 2009;273:194–200.
34. Medina M, Wandosell F. Deconstructing GSK-3: The Fine Regulation of Its Activity. Int J Alzheimer's Dis 2011;2011:479249.
35. Mavila N, James D, Utley S, Cu N, Coblens O, Mak K, et al. Fibroblast growth factor receptor-mediated activation of AKT-beta-catenin-CBP pathway regulates survival and proliferation of murine hepatoblasts and hepatic tumor initiating stem cells. PLoS One 2012;7:e50401.
36. Wiza C, Nascimento EB, Ouwens DM. Role of PRAS40 in Akt and mTOR signaling in health and disease. Am J Physiol Endocrinol Metab 2012;302:E1453–60.
37. Vander Haar E, Lee SI, Bandhakavi S, Griffin TJ, Kim DH. Insulin signalling to mTOR mediated by the Akt/PKB substrate PRAS40. Nat Cell Biol 2007;9:316–23.
38. Herrera-Abreu MT, Pearson A, Campbell J, Shnyder SD, Knowles MA, Ashworth A, et al. Parallel RNA interference screens identify EGFR activation as an escape mechanism in FGFR3-mutant cancer. Cancer Discov 2013;3:1058–71.
39. Terai H, Soejima K, Yasuda H, Nakayama S, Hamamoto J, Arai D, et al. Activation of the FGF2-FGFR1 autocrine pathway: a novel mechanism of acquired resistance to gefitinib in NSCLC. Mol Cancer Res 2013;11:759–67.

Published OnlineFirst March 2, 2017; DOI: 10.1158/1535-7163.MCT-15-1010



40. Wang J, Mikse O, Liao RG, Li Y, Tan L, Janne PA, et al. Ligand-associated ERBB2/3 activation confers acquired resistance to FGFR inhibition in FGFR3-dependent cancer cells. Oncogene 2015;34:2167–77.
41. Harbinski F, Craig VJ, Sanghavi S, Jeffery D, Liu L, Sheppard KA, et al. Rescue screens with secreted proteins reveal compensatory potential of receptor tyrosine kinases in driving cancer growth. Cancer Discov 2012;2:948–59.
42. Chell V, Balmanno K, Little AS, Wilson M, Andrews S, Blockley L, et al. Tumour cell responses to new fibroblast growth factor receptor tyrosine kinase inhibitors and identification of a gatekeeper mutation in FGFR3 as a mechanism of acquired resistance. Oncogene 2013;32:3059–70.
43. Hu Y, Lu H, Zhang J, Chen J, Chai Z, Zhang J. Essential role of AKT in tumor cells addicted to FGFR. Anticancer Drugs 2014;25:183–8.
44. Grygielewicz P, Dymek B, Bujak A, Gunerka P, Stanczak A, Lamparska-Przybysz M, et al. Epithelial-mesenchymal transition confers resistance to selective FGFR inhibitors in SNU-16 gastric cancer cells. Gastric Cancer 2016;19:53–62.
45. Takata M, Chikumi H, Miyake N, Adachi K, Kanamori Y, Yamasaki A, et al. Lack of AKT activation in lung cancer cells with EGFR mutation is a novel marker of cetuximab sensitivity. Cancer Biol Ther 2012; 13:369–78.
46. Russo M, Misale S, Wei G, Siravegna G, Crisafulli G, Lazzari L, et al. Acquired resistance to the TRK inhibitor entrectinib in colorectal cancer. Cancer Discov 2016;6:36–44.
47. Siravegna G, Mussolin B, Buscarino M, Corti G, Cassingena A, Crisafulli G, et al. Clonal evolution and resistance to EGFR blockade in the blood of colorectal cancer patients. Nat Med 2015;21:795–801.
48. Flaherty KT, Infante JR, Daud A, Gonzalez R, Kefford RF, Sosman J, et al. Combined BRAF and MEK inhibition in melanoma with BRAF V600 mutations. N Engl J Med 2012;367:1694–703.
49. Baselga J, Campone M, Piccart M, Burris HA 3rd, Rugo HS, Sahmoud T, et al. Everolimus in postmenopausal hormone-receptor-positive advanced breast cancer. N Engl J Med 2012;366:520–9.

Published OnlineFirst March 2, 2017; DOI: 10.1158/1535-7163.MCT-15-1010



Molecular Cancer Therapeutics

# Akt Activation Mediates Acquired Resistance to Fibroblast Growth Factor Receptor Inhibitor BGJ398

Jharna Datta, Senthilkumar Damodaran, Hannah Parks, et al.

*Mol Cancer Ther* 2017;16:614-624. Published OnlineFirst March 2, 2017.